

Constructive molecular configurations for surface-defect passivation of perovskite photovoltaics

5 Rui Wang^{1†}, Jingjing Xue^{1†*}, Kai-Li Wang^{2†}, Zhao-Kui Wang^{1,2*}, Yanqi Luo³, David Fenning³,
Guangwei Xu¹, Selbi Nuryyeva^{1,5}, Tianyi Huang¹, Yepin Zhao¹, Jonathan Lee Yang¹, Jiahui Zhu¹,
Minhuan Wang¹, Shaun Tan¹, Ilhan Yavuz^{4*}, Kendall N. Houk^{5*} and Yang Yang^{1,6*}

¹Department of Materials Science and Engineering and California NanoSystems Institute, University of California Los Angeles, CA 90095, USA

10 ²Institute of Functional Nano & Soft Materials (FUNSOM), Jiangsu Key Laboratory for Carbon-Based Functional Materials & Devices, Soochow University, Suzhou 215123, China

³Department of Nanoengineering, University of California, San Diego, La Jolla, CA 92093, USA

⁴Department of Physics, Marmara University, 34722, Ziverbey, Istanbul, Turkey

⁵Department of Chemistry and Biochemistry, University of California Los Angeles, CA 90095, USA

15 ⁶School of Engineering, Westlake University, Hangzhou 310024, China

*Correspondence and requests for materials should be addressed to J.X. (email: jjxue@ucla.edu) or to
20 Z.K.W (email: zkwang@suda.edu.cn) or to I.Y. (email: ilhan.yavuz@marmara.edu.tr) or to K.H. (email:
houk@chem.ucla.edu) or to Y.Y. (email: yangy@ucla.edu)

†These authors contributed equally to this work

Abstract:

Surface trap-mediated non-radiative charge recombination is a major limit to achieving high-efficiency metal-halide perovskite photovoltaics. The ionic character of perovskite lattice has enabled molecular defect passivation approaches via interaction between functional groups and defects. However, a lack of in-depth understanding of how the molecular configuration influence the passivation effectiveness is a challenge to rational molecule design. Here, the chemical environment of a functional group that is activated for defect passivation was systematically investigated with theophylline, caffeine and theobromine. When N-H and C=O were in an optimal configuration within the molecule, hydrogen-bond formation between N-H and I assisted the primary C=O binding with the antisite Pb defect to maximize surface-defect binding. A stabilized power conversion efficiency of 22.6% of photovoltaic device was demonstrated with theophylline treatment.

Defect passivation to reduce unproductive charge recombination is an effective strategy to increase the power conversion efficiency (PCE) of polycrystalline metal-halide perovskite thin-film photovoltaics (PVs) (6–11). The ionic nature of the perovskite lattice enables molecular passivation through coordinate binding based on Lewis acid-base chemistry (12–15). Several organic molecules containing functional groups that can passivate defects (16–18), such as carbonyl groups (19, 20). The selection of molecules with optimal binding configurations for defect passivation would benefit from molecular design rules (21, 22).

We demonstrate high efficiencies for $(\text{FAPbI}_3)_x(\text{MAPbBr}_3)_{1-x}$ (where FA is formamidinium and MA is methylammonium, x is 0.92 in the precursor) perovskite PV devices through defect identification (23) followed by rational design and comprehensive investigation of the chemical environment around the active functional group for defect passivation. In high-quality perovskite polycrystalline thin films that have monolayered grains (24–26), interior defects of perovskite are negligible compared to the surface defects. We used density-functional theory (DFT) calculations to compare the formation energies of selected native defects on the perovskite surface. Particularly taken into consideration were Pb- and I-involving point defects, Pb vacancy (V_{Pb}), I vacancy (V_{I}) and Pb-I antisite (Pb_{I} and I_{Pb} , corresponding to I site substitution by Pb, and Pb site substitution by I, respectively) because the band edges of perovskite were reported to be composed of Pb and I orbitals (27, 28).

As confirmed by x-ray photoelectron spectroscopy (XPS), the surface of the as-fabricated perovskite thin film synthesized by a two-step method was Pb-rich (Fig. S1), and we focused on the (100) surface with PbI_2 termination in a Pb-rich condition. The types of surface defects studied, and their corresponding top layer view of atomic structures (Fig. 1A). The defect formation energies (DFEs) we calculated using PDE-D3 method (Table S1) of V_{Pb} , V_{I} , Pb_{I} , and I_{Pb} on the surface were 3.20, 0.51, 0.57, and 3.15 eV, respectively. Compared to the values reported in bulk perovskite, V_{Pb} , V_{I} and I_{Pb} defects show similar DFEs (29), whereas the Pb_{I} antisite defect exhibited particularly lower formation energy than that in the bulk. Thus, the Pb_{I} antisite defect should form more readily and predominate on the surface. We did not consider V_{I} further despite its DFE being as low as that of Pb_{I} because the interaction of molecules with the V_{I} turned out to be not energy favorable (Fig. S2).

Based on these results, we focused on the interaction between the surface Pb_{I} antisite defect and candidate molecules for defect passivation. A set of small molecules sharing the identical functional groups but with strategically varying chemical structure were investigated, namely

theophylline, caffeine, and theobromine, interacting with the defects (Fig. 1B). These molecules are found in natural products (tea, coffee and chocolate, respectively) and are readily accessible. In these molecules, the conjugated structure as well as the dipoles induced by the hetero atoms tend to increase the intermolecular interaction. This renders them non-volatile in nature, which is key to the investigation of their interactions with defects in perovskite and long-term stability of the devices. The xanthine core also helps maintain the coplanarity of the carbonyl group and the N-H. Unlike other small molecules with flexible alkyl chains, this rigidity allows us to define the configuration and distance between the carbonyl group and N-H when they are interacting with the defects, as a result of which the constructive molecular configuration for defect passivation can be unraveled.

We incorporated theophylline onto the surface of perovskite thin film using a post-treatment method, and a PCE enhancement from 21.02% (stabilized 20.36%) to 23.48% (stabilized 22.64%) was observed in the photovoltaic devices with ITO/SnO₂/perovskite/Spiro-OMeTAD/Ag structure under reverse scan direction (where ITO is indium tin oxide, SnO₂ is tin oxide and Spiro-OMeTAD is 2,2',7,7'-tetrakis-(N,N-di-p-methoxyphenyl amine)-9,9'-spirobifluorene), current density-voltage (*J-V*) curves of the PV devices with and without theophylline treatment are compared in Fig. 1C and Table S2. The control device showed an open circuit voltage (*V*_{OC}) of 1.164 V, a short circuit current (*J*_{SC}) of 24.78 mA cm⁻², a fill factor (FF) of 72.88%, whereas the target device showed a *V*_{OC} of 1.191 V, a *J*_{SC} of 25.24 mA cm⁻², a FF of 78.11%. The enhancement in the *V*_{OC} we attributed to the surface passivation by theophylline through the Lewis base-acid interaction between C=O group and the antisite Pb. As shown in the surface structure model of perovskite with theophylline (Fig. 1B), the C=O group on theophylline strongly interacted with the antisite Pb. The neighboring N-H on the imidazole ring also interacted with the I of PbI₆²⁻ octahedron through a hydrogen bond (H-bond), which strengthened the absorption of theophylline onto the Pb_I defect, resulting in an interaction energy (*E*_{int}, defined as *E*_{molecule-perovskite} - *E*_{perovskite} - *E*_{molecule}) as strong as -1.7 eV.

This observation suggested that the neighboring H-bond between the xanthine molecule and the PbI₆²⁻ octahedron can contribute to the defect passivation. A methyl group was added to the N on the imidazole ring of theophylline (resulting in caffeine) to eliminate the effect from H-bonding between the N-H and I and leaving just the interaction with surface Pb_I defects (Fig. 1B). The missing H-bond between N-H and PbI₆²⁻ octahedron resulted in a weakened interaction and a less favorable *E*_{int} of -1.3 eV. Compare with the theophylline-treated device, a caffeine-treated perovskite PV device had a lower PCE of 22.32% along with a lower *V*_{OC} of 1.178 V, *J*_{SC} of 25.04 mA cm⁻², and FF of 75.76%.

When the N-H group was located next to the C=O group on the same six-membered ring, producing a shorter distance between the C=O and the N-H, in theobromine, the spatially effective interaction between the N-H and I was disabled as C=O was bound to antisite Pb, resulting in an even weaker interaction energy of -1.1 eV (Fig. 1B). Although both C=O and N-H are both present on the molecule, the lack of appropriate coordination of I to the molecule led to a spatially destructive molecular configuration. The theobromine-treated devices showed a decrease in PCE to 20.24% with a lower *V*_{OC} of 1.163 V, *J*_{SC} of 24.27 mA cm⁻² and FF of 71.58% compared with the reference device. This result emphasizes the importance of the constructive configuration of N-H and C=O groups that enable the cooperative multisite interaction and synergistic passivation effect.

We studied the variation in the C=O and the PbI₂-terminated perovskite surface interaction with different molecular configurations using Fourier-transform infrared spectroscopy (FTIR). The C=O in pure theophylline showed a typical stretching vibration mode at 1660 cm⁻¹ that it shifted to 1630 cm⁻¹ upon binding to PbI₂ (Fig. 2A). The downward shift of 30 cm⁻¹ of the C=O stretching vibration frequency resulted from the electron delocalization in C=O when a Lewis base-acid adduct was formed, demonstrating a strong interaction between PbI₂ and C=O in theophylline. The atomic distance between the O in C=O and the Pb in PbI₂ based on theoretical modeling was as low as 2.28 Å.

When the H atom was replaced by a methyl group on the N of imidazole to eliminate the effect of a H-bond, the vibration frequency of C=O in caffeine shifted only 10 cm⁻¹ upon addition of PbI₂, indicating a weakened interaction between the C=O and PbI₂ (Fig. 2B). The atomic distance between the corresponding O and Pb also increased to 2.32 Å. In the case of theobromine, when the N-H was in a closer position to C=O, the interaction between the molecule and PbI₂ became comparable to that in theophylline, as evidenced by the large shift of C=O stretching vibration frequency from 1655 to 1620 cm⁻¹ and the short distance between O and Pb (Fig. 2C). However, this strong interaction was enabled by the free rotation of PbI₂, which resulted in a different configuration than that in theophylline and caffeine. Hence, when the configuration of PbI₂ was fixed and had a 90° angle between Pb and I atom, like that on perovskite surface (the PbI₆²⁻ octahedron), the N-H was in a position that led to an unfavorable interaction with I. This configuration would either cause weakened interaction between the molecule and the perovskite surface or distorted PbI₆²⁻ octahedron, resulting in the ineffectiveness of defect passivation and perhaps causing even more defects through lattice distortion (Fig. S3).

The surface passivation effects of the three molecules with different configuration were further studied by photoluminescence (PL). The PL intensity increased noticeably with the treatment by theophylline (Fig. 2D), implying the suppressed nonradiative charge recombination sites from defects(20). With the caffeine treatment, enhanced PL intensity was also observed, but not as strong as that with the theophylline, suggesting a less effective passivation effect. For theobromine, however, a decrease in PL intensity was observed compared with the reference material, which can be attributed to the destructive molecular configuration of the passivation agents causing more charge recombination sites.

The trap density of states (*t*DOS) of the as-fabricated devices were also deduced from the angular frequency-dependent capacitance. As shown in Fig. 2E, the *t*DOS as a function of the defect energy demonstrated a reduction in trap states for theophylline- and caffeine- treated perovskite compared with the reference device. In contrast, theobromine treatment induced more trap states, consistent with the decrease in PCE. The change in *t*DOS with different surface treatments was also confirmed by theoretical modeling (Fig. S4). In addition, electrochemical impedance spectroscopy (EIS) characterization was performed to demonstrate the carrier transport processes under illumination at the interface. The middle frequency zone of EIS semicircle should be dominated by junction capacitance and recombination resistance related to the interfaces between transport materials and perovskite. According to Fig. 2F, the device with theophylline surface treatment has the smallest impedance, signifying a substantially suppressed charge recombination at the interface, which originated from the reduced surface defect states. A larger impedance was observed in caffeine-treated device and an even larger impedance was measured in theobromine-treated device.

Further characterizations were performed to better understand the perovskite interface with theophylline. High-resolution XPS patterns of the Pb 4*f* for the theophylline-treated film showed two main peaks located at 138.48 and 143.38 eV, corresponding to the Pb 4*f* 7/2 and Pb 4*f* 5/2, respectively (Fig. 3A), where the reference film showed two main peaks at 138.27 and 143.13 eV. The peaks from Pb 4*f* shifted to higher binding energies in the film with theophylline surface treatment, indicating the interaction between the theophylline and the Pb on perovskite surface. We used ultraviolet photoelectron spectroscopy (UPS) to measure the surface band structure with and without the theophylline surface treatment. The work function was determined to be -4.77 eV and -4.96 eV with the valance band maximum (VBM) of -5.66 and -5.73 eV for reference and theophylline, respectively (Fig. 3B). This difference indicated a less n-type surface after theophylline treatment, which could improve the hole extraction in devices.

Atomic force microscopy combined with Kelvin probe force microscopy (KPFM) was further applied to probe the effect of theophylline on the surface morphology and surface potential. The theophylline-treated surface exhibited a higher electronic chemical potential than that of reference film, while keeping the surface morphology unchanged (Fig. 3C). The transient photoluminescence (TRPL) of the perovskite films with hole-transporting layer (HTL) was compared in Fig. 3D to delineate the carrier dynamics of the devices. The perovskite film with theophylline treatment showed a slightly longer carrier lifetime than the reference film, whereas a faster decay profile was observed when adding the HTL on top of the perovskite film. This result demonstrated a better hole extraction with theophylline treatment (25), most likely arising from lesser recombination sites at the interface and the slightly shallower work function of the perovskite film with theophylline.

The improved carrier dynamics originating from the effective surface passivation by theophylline was further characterized by cross-sectional electron-beam-induced current (EBIC) measurement. In EBIC measurement, the electron-beam excited carriers were collected based on the collection probability $CP(x, L_d)$, where x is the distance between junction and incident beam position, and L_d is the diffusion length of the carriers (Fig. S5). The device with theophylline treatment exhibited higher EBIC current compared to the reference device (Fig. 3E). The average intensity extracted from these EBIC maps demonstrated a general increase in the EBIC signal after treated with theophylline (Fig. S6), indicating an enhanced carrier collection efficiency (30). Specifically, in Fig. 3E, a representative EBIC line profile of the reference device showed a current decay from the HTL/perovskite to the SnO₂/perovskite interface. The decay indicates that carrier collection was limited by the hole-diffusion length as the beam position moved away from the HTL/perovskite interface. In contrast, the device with theophylline treatment displays minimal decay within the perovskite layer in the EBIC line profile. This difference suggests that a longer diffusion length of holes was present in theophylline-treated sample and balanced electron and hole charge transport and collection was achieved, which is likely the result of fewer surface recombination sites (Fig. 3E).

Further assessment of the performance of the PV devices based on the theophylline surface passivation was performed. The devices showed a negligible hysteresis (4.1%, Fig. 4A) because of the balanced charge collection originated from the effective surface passivation, whereas the reference device showed a large hysteresis (up to 7.6%, Table S3). External quantum efficiency (EQE) spectra of the devices were compared in Fig. 4B. An integrated J_{SC} of 24.42 mA cm⁻² from the target device matched well with the value measured from the J - V scan (<5% discrepancy), whereas the control device showed an integrated J_{SC} of 23.56 mA cm⁻². A stabilized PCE of

22.64% was achieved with the target device when biased at 1.00 V while that of control device was 20.36% when biased at 0.98 V (Fig. 4C). The histogram of PV efficiencies for 40 devices is shown in Fig. 4D (the detailed parameters are shown in Table S2), which confirms good reproducibility of the performance improvement with theophylline (11.1% improvement in an average PCE from $20.36 \pm 0.53\%$ to $22.61 \pm 0.58\%$ with the incorporation of the theophylline).

The changes in PCE of the encapsulated devices at a relative humidity of 30 to 40% and temperature of 40 °C were tracked over time to test the long-term operational stability (Fig. 4E). The reference device (initial PCE 19.34%) degraded by more than 80% in 500 hours, whereas the target device maintained > 90% of its initial efficiency (21.32%) during this time. Also, as shown in Fig. S7, the shelf stability of the device based on theophylline treatment was noticeably enhanced, maintaining over 95% of its original PCE (22.78%) when stored under ambient conditions with 20 to 30% humidity at 25 °C for 60 days. In contrast, the reference device lost > 35% of its initial efficiency (20.67%). The strong interaction between the theophylline and the surface defects likely suppressed deleterious ion migration (31–33).

References and Notes:

1. H. S. Kim, C. R. Lee, J. H. Im, K. B. Lee, T. Moehl, A. Marchioro, S. J. Moon, R. Humphry-Baker, J. H. Yum, J. E. Moser, M. Grätzel, N. G. Park, Lead iodide perovskite sensitized all-solid-state submicron thin film mesoscopic solar cell with efficiency exceeding 9%. *Sci. Rep.* **2**, 591 (2012).
2. S. D. Stranks, H. J. Snaith, Metal-halide perovskites for photovoltaic and light-emitting devices. *Nat. Nanotechnol.* **10**, 391–402 (2015).
3. H. Zhu, K. Miyata, Y. Fu, J. Wang, P. P. Joshi, D. Niesner, K. W. Williams, S. Jin, X. Y. Zhu, Screening in crystalline liquids protects energetic carriers in hybrid perovskites. *Science*. **353**, 1409–1413 (2016).
4. M. Xiao, F. Huang, W. Huang, Y. Dkhissi, Y. Zhu, J. Etheridge, A. Gray-Weale, U. Bach, Y. B. Cheng, L. Spiccia, A fast deposition-crystallization procedure for highly efficient lead iodide perovskite thin-film solar cells. *Angew. Chemie - Int. Ed.* **53**, 9898–9903 (2014).
5. W. Nie, H. Tsai, R. Asadpour, J. C. Blancon, A. J. Neukirch, G. Gupta, J. J. Crochet, M. Chhowalla, S. Tretiak, M. A. Alam, H. L. Wang, A. D. Mohite, High-efficiency solution-processed perovskite solar cells with millimeter-scale grains. *Science*. **347**, 522–525 (2015).
6. J. Tong, Z. Song, D. H. Kim, X. Chen, C. Chen, A. F. Palmstrom, P. F. Ndione, M. O. Reese, S. P. Dunfield, O. G. Reid, J. Liu, F. Zhang, S. P. Harvey, Z. Li, S. T. Christensen, G. Teeter, D. Zhao, M. M. Al-Jassim, M. F. A. M. Van Hest, M. C. Beard, S. E. Shaheen, J. J. Berry, Y. Yan, K. Zhu, Carrier lifetimes of >1 μ s in Sn-Pb perovskites enable efficient all-perovskite tandem solar cells. *Science*. **364**, 475–479 (2019).
7. H. Tan, A. Jain, O. Voznyy, X. Lan, F. P. G. De Arquer, J. Z. Fan, R. Quintero-Bermudez, M. Yuan, B. Zhang, Y. Zhao, F. Fan, P. Li, L. N. Quan, Y. Zhao, Z. H. Lu, Z. Yang, S. Hoogland, E. H. Sargent, Efficient and stable solution-processed planar perovskite solar cells via contact passivation. *Science*. **355**, 722–726 (2017).
8. X. Zheng, B. Chen, J. Dai, Y. Fang, Y. Bai, Y. Lin, H. Wei, X. C. Zeng, J. Huang, Defect passivation in hybrid perovskite solar cells using quaternary ammonium halide anions and cations. *Nat. Energy*. **2**, 17102 (2017).

9. J. J. Yoo, S. Wieghold, M. Sponseller, M. Chua, S. N. Bertram, N. T. P. Hartono, J. Tresback, E. Hansen, J.-P. Correa-Baena, V. Bulovic, T. Buonassisi, S. S. Shin, M. G. Bawendi, An Interface Stabilized Perovskite Solar Cell with High Stabilized Efficiency and Low Voltage Loss. *Energy Environ. Sci.* **12**, 2192–2199 (2019).
- 5 10. Q. Jiang, Y. Zhao, X. Zhang, X. Yang, Y. Chen, Z. Chu, Q. Ye, X. Li, Z. Yin, J. You, Surface passivation of perovskite film for efficient solar cells. *Nat. Photonics.* **13**, 460–466 (2019).
- 10 11. N. Li, S. Tao, Y. Chen, X. Niu, C. K. Onwudinanti, C. Hu, Z. Qiu, Z. Xu, G. Zheng, L. Wang, Y. Zhang, L. Li, H. Liu, Y. Lun, J. Hong, X. Wang, Y. Liu, H. Xie, Y. Gao, Y. Bai, S. Yang, G. Brocks, Q. Chen, H. Zhou, Cation and anion immobilization through chemical bonding enhancement with fluorides for stable halide perovskite solar cells. *Nat. Energy.* **4**, 408–415 (2019).
12. J. S. Manser, J. A. Christians, P. V. Kamat, Intriguing Optoelectronic Properties of Metal Halide Perovskites. *Chem. Rev.* **116**, 12956–13008 (2016).
- 15 13. H. Zhang, H. Chen, C. C. Stoumpos, J. Ren, Q. Hou, X. Li, J. Li, H. He, H. Lin, J. Wang, F. Hao, M. G. Kanatzidis, Thiazole-Induced Surface Passivation and Recrystallization of CH₃NH₃PbI₃ Films for Perovskite Solar Cells with Ultrahigh Fill Factors. *ACS Appl. Mater. Interfaces.* **10**, 42436–42443 (2018).
- 20 14. J. W. Lee, H. S. Kim, N. G. Park, Lewis Acid-Base Adduct Approach for High Efficiency Perovskite Solar Cells. *Acc. Chem. Res.* **49**, 311–319 (2016).
15. Y. Zong, Y. Zhou, Y. Zhang, Z. Li, L. Zhang, M. G. Ju, M. Chen, S. Pang, X. C. Zeng, N. P. Padture, Continuous Grain-Boundary Functionalization for High-Efficiency Perovskite Solar Cells with Exceptional Stability. *Chem.* **4**, 1404–1415 (2018).
- 25 16. D. Bi, C. Yi, J. Luo, J. D. Décoppet, F. Zhang, S. M. Zakeeruddin, X. Li, A. Hagfeldt, M. Grätzel, Polymer-templated nucleation and crystal growth of perovskite films for solar cells with efficiency greater than 21%. *Nat. Energy.* **1**, 16142 (2016).
17. B. Chen, P. N. Rudd, S. Yang, Y. Yuan, J. Huang, Imperfections and their passivation in halide perovskite solar cells. *Chem. Soc. Rev.* **48**, 3842–3867 (2019).
- 30 18. T. Wu, Y. Wang, X. Li, Y. Wu, X. Meng, D. Cui, X. Yang, L. Han, Efficient Defect Passivation for Perovskite Solar Cells by Controlling the Electron Density Distribution of Donor- π -Acceptor Molecules. *Adv. Energy Mater.* **9**, 1803766 (2019).
19. T. Niu, J. Lu, R. Munir, J. Li, D. Barrit, X. Zhang, H. Hu, Z. Yang, A. Amassian, K. Zhao, S. F. Liu, Stable High-Performance Perovskite Solar Cells via Grain Boundary Passivation. *Adv. Mater.* **30**, 1706576 (2018).
- 35 20. R. Wang, J. Xue, L. Meng, J. W. Lee, Z. Zhao, P. Sun, L. Cai, T. Huang, Z. Wang, Z. K. Wang, Y. Duan, J. L. Yang, S. Tan, Y. Yuan, Y. Huang, Y. Yang, Caffeine Improves the Performance and Thermal Stability of Perovskite Solar Cells. *Joule.* **3**, 1464–1477 (2019).
- 40 21. W. Xu, Q. Hu, S. Bai, C. Bao, Y. Miao, Z. Yuan, T. Borzda, A. J. Barker, E. Tyukalova, Z. Hu, M. Kawecki, H. Wang, Z. Yan, X. Liu, X. Shi, K. Uvdal, M. Fahlman, W. Zhang, M. Duchamp, J. M. Liu, A. Petrozza, J. Wang, L. M. Liu, W. Huang, F. Gao, Rational molecular passivation for high-performance perovskite light-emitting diodes. *Nat.*

- Photonics*. **13**, 418–424 (2019).
22. H. Zhang, M. K. Nazeeruddin, W. C. H. Choy, Perovskite Photovoltaics: The Significant Role of Ligands in Film Formation, Passivation, and Stability. *Adv. Mater.* **31**, 1805702 (2019).
- 5 23. W. J. Yin, T. Shi, Y. Yan, Unusual defect physics in CH₃NH₃PbI₃ perovskite solar cell absorber. *Appl. Phys. Lett.* **104**, 063903 (2014).
24. W. S. Yang, B. W. Park, E. H. Jung, N. J. Jeon, Y. C. Kim, D. U. Lee, S. S. Shin, J. Seo, E. K. Kim, J. H. Noh, S. Il Seok, Iodide management in formamidinium-lead-halide-based perovskite layers for efficient solar cells. *Science*. **356**, 1376–1379 (2017).
- 10 25. N. J. Jeon, H. Na, E. H. Jung, T. Y. Yang, Y. G. Lee, G. Kim, H. W. Shin, S. Il Seok, J. Lee, J. Seo, A fluorene-terminated hole-transporting material for highly efficient and stable perovskite solar cells. *Nat. Energy*. **3**, 682–689 (2018).
26. E. H. Jung, N. J. Jeon, E. Y. Park, C. S. Moon, T. J. Shin, T. Y. Yang, J. H. Noh, J. Seo, Efficient, stable and scalable perovskite solar cells using poly(3-hexylthiophene). *Nature*. **567**, 511–515 (2019).
- 15 27. M. A. Green, A. Ho-Baillie, H. J. Snaith, The emergence of perovskite solar cells. *Nat. Photonics*. **8**, 506–514 (2014).
28. Z. Xiao, Z. Song, Y. Yan, From Lead Halide Perovskites to Lead-Free Metal Halide Perovskites and Perovskite Derivatives. *Adv. Mater.*, 1803792 (2019).
- 20 29. N. Liu, C. Y. Yam, First-principles study of intrinsic defects in formamidinium lead triiodide perovskite solar cell absorbers. *Phys. Chem. Chem. Phys.* **20**, 6800–6804 (2018).
30. E. Edri, S. Kirmayer, S. Mukhopadhyay, K. Gartsman, G. Hodes, D. Cahen, Elucidating the charge carrier separation and working mechanism of CH₃NH₃PbI_{3-x}Cl_x perovskite solar cells. *Nat. Commun.* **5**, 3461 (2014).
- 25 31. R. Wang, M. Mujahid, Y. Duan, Z. K. Wang, J. Xue, Y. Yang, A Review of Perovskites Solar Cell Stability. *Adv. Funct. Mater.*, 1808843 (2019).
32. J. A. Christians, P. Schulz, J. S. Tinkham, T. H. Schloemer, S. P. Harvey, B. J. Tremolet De Villers, A. Sellinger, J. J. Berry, J. M. Luther, Tailored interfaces of unencapsulated perovskite solar cells for >1,000 hour operational stability. *Nat. Energy*. **3**, 68–74 (2018).
- 30 33. Y. Hou, X. Du, S. Scheiner, D. P. McMeekin, Z. Wang, N. Li, M. S. Killian, H. Chen, M. Richter, I. Levchuk, N. Schrenker, E. Spiecker, T. Stubhan, N. A. Luechinger, A. Hirsch, P. Schmuki, H. P. Steinrück, R. H. Fink, M. Halik, H. J. Snaith, C. J. Brabec, A generic interface to reduce the efficiency-stability-cost gap of perovskite solar cells. *Science*. **358**, 1192–1197 (2017).
- 35 34. G. Kresse, J. Furthmüller, Efficiency of ab-initio total energy calculations for metals and semiconductors using a plane-wave basis set. *Comput. Mater. Sci.* **6**, 15–50 (1996).
- 35 35. G. Kresse, J. Furthmüller, Efficient iterative schemes for ab initio total-energy calculations using a plane-wave basis set. *Phys. Rev. B - Condens. Matter Mater. Phys.* **54**, 11169–11186 (1996).
- 40 36. J. P. Perdew, K. Burke, M. Ernzerhof, Generalized gradient approximation made simple.

Phys. Rev. Lett. **77**, 3865–3868 (1996).

37. J. P. Perdew, A. Ruzsinszky, G. I. Csonka, O. A. Vydrov, G. E. Scuseria, L. A. Constantin, X. Zhou, K. Burke, Restoring the Density-Gradient Expansion for Exchange in Solids and Surfaces. *Phys. Rev. Lett.* **100**, 136406 (2008).
- 5 38. S. Grimme, J. Antony, S. Ehrlich, H. Krieg, A consistent and accurate ab initio parametrization of density functional dispersion correction (DFT-D) for the 94 elements H-Pu. *J. Chem. Phys.* **132**, 154104 (2010).
39. S. Grimme, Semiempirical GGA-type density functional constructed with a long-range dispersion correction. *J. Comput. Chem.* **27**, 1787–1799 (2006).
- 10 40. P. E. Blöchl, Projector augmented-wave method. *Phys. Rev. B.* **50**, 17953–17979 (1994).
41. G. I. Csonka, J. P. Perdew, A. Ruzsinszky, P. H. T. Philipsen, S. Lebègue, J. Paier, O. A. Vydrov, J. G. Ángyán, Assessing the performance of recent density functionals for bulk solids. *Phys. Rev. B - Condens. Matter Mater. Phys.* **79**, 155107 (2009).
- 15 42. Gaussian 16, Revision A.03, Frisch, M. J.; Trucks, G. W.; Schlegel, H. B.; Scuseria, G. E.; Robb, M. A.; Cheeseman, J. R.; Scalmani, G.; Barone, V.; Petersson, G. A.; Nakatsuji, H.; Li, X.; Caricato, M.; Marenich, A. V.; Bloino, J.; Janesko, B. G.; Gomperts, R.; Mennucci, B.; Hratchian, H. P.; Ortiz, J. V.; Izmaylov, A. F.; Sonnenberg, J. L.; Williams-Young, D.; Ding, F.; Lipparini, F.; Egidi, F.; Goings, J.; Peng, B.; Petrone, A.; Henderson, T.; Ranasinghe, D.; Zakrzewski, V. G.; Gao, J.; Rega, N.; Zheng, G.; Liang, W.; Hada, M.; Ehara, M.; Toyota, K.; Fukuda, R.; Hasegawa, J.; Ishida, M.; Nakajima, T.; Honda, Y.; Kitao, O.; Nakai, H.; Vreven, T.; Throssell, K.; Montgomery, J. A., Jr.; Peralta, J. E.; Ogliaro, F.; Bearpark, M. J.; Heyd, J. J.; Brothers, E. N.; Kudin, K. N.; Staroverov, V. N.; Keith, T. A.; Kobayashi, R.; Normand, J.; Raghavachari, K.; Rendell, A. P.; Burant, J. C.; Iyengar, S. S.; Tomasi, J.; Cossi, M.; Millam, J. M.; Klene, M.; Adamo, C.; Cammi, R.; Ochterski, J. W.; Martin, R. L.; Morokuma, K.; Farkas, O.; Foresman, J. B.; Fox, D. J. Gaussian, Inc., Wallingford CT, (2016).
- 20 43. CYLview, 1.0b; Legault, C. Y., Université de Sherbrooke, (2009) (<http://www.cylview.org>)
44. M. T. Weller, O. J. Weber, J. M. Frost, A. Walsh, Cubic Perovskite Structure of Black Formamidinium Lead Iodide, α -[HC(NH₂)₂]PbI₃, at 298 K. *J. Phys. Chem. Lett.* **6**, 3209–3212 (2015).
- 30 45. C. Ran, J. Xu, W. Gao, C. Huang, S. Dou, Defects in metal triiodide perovskite materials towards high-performance solar cells: Origin, impact, characterization, and engineering. *Chem. Soc. Rev.* **47** (2018), 4581–4610.
46. H. Uratani, K. Yamashita, Charge Carrier Trapping at Surface Defects of Perovskite Solar Cell Absorbers: A First-Principles Study. *J. Phys. Chem. Lett.* **8**, 742–746 (2017).
- 35

Acknowledgement:

40 **Funding:** Y.Y. acknowledged the Office of Naval Research (ONR) (N00014-17-1-2,484) for their financial support. Part of this material is based upon work supported by the U.S. Department of

Energy's Office of Energy Efficiency and Renewable Energy (EERE) under the Solar Energy Technologies Office Award Number DE- EE0008751. And Z.K.W. acknowledged the Natural Science Foundation of China (No. 91733301). This project was also supported by the Collaborative Innovation Center of Suzhou Nano Science and Technology. Y.L. and D.F. are grateful for the financial support of a California Energy Commission Advance Breakthrough award (EPC-16-050). This work was performed in part at the San Diego Nanotechnology Infrastructure (SDNI) of UCSD supported by the National Science Foundation (Grant ECCS-1542148). Part of the computations are performed in the SIMULAB of Marmara University, Physics Department and in the UHEM cluster of Turkey. K.N.H. and S.N. are grateful to the National Science Foundation (CHE-1764328) for financial support of this research. Computer time was provided by the UCLA Institute for Digital Research and Education (IDRE). **Author contributions:** R.W., J.X., and Y.Y. conceived the idea. R.W. and J.X. fabricated the solar cell devices and designed the experiments. K.L.W. performed the film and device characterizations under the supervision of Z.K.W.. Y.L. and D.F. performed the EBIC measurement. G.X. carried out the t DOS measurement. S.N., I.Y., and K.N.H. performed the DFT calculation. T.H. carried out the TPC and TPV measurement. Y.Z., J.L.Y., J.Z., M.W. and S.T. assisted with the device fabrication and characterizations. R.W., J.X., and Y.Y. wrote the manuscript. All the authors discussed the results and commented on the manuscript. Y.Y. supervised the project. **Competing interests:** None declared. **Data and materials availability:** All (other) data needed to evaluate the conclusions in the paper are present in the paper or the Supplementary Materials.

Supplementary Materials:

Materials and Methods

Supplementary Text

Figs S1-S13

Tables S1-S3

References (23,29, 34-46)

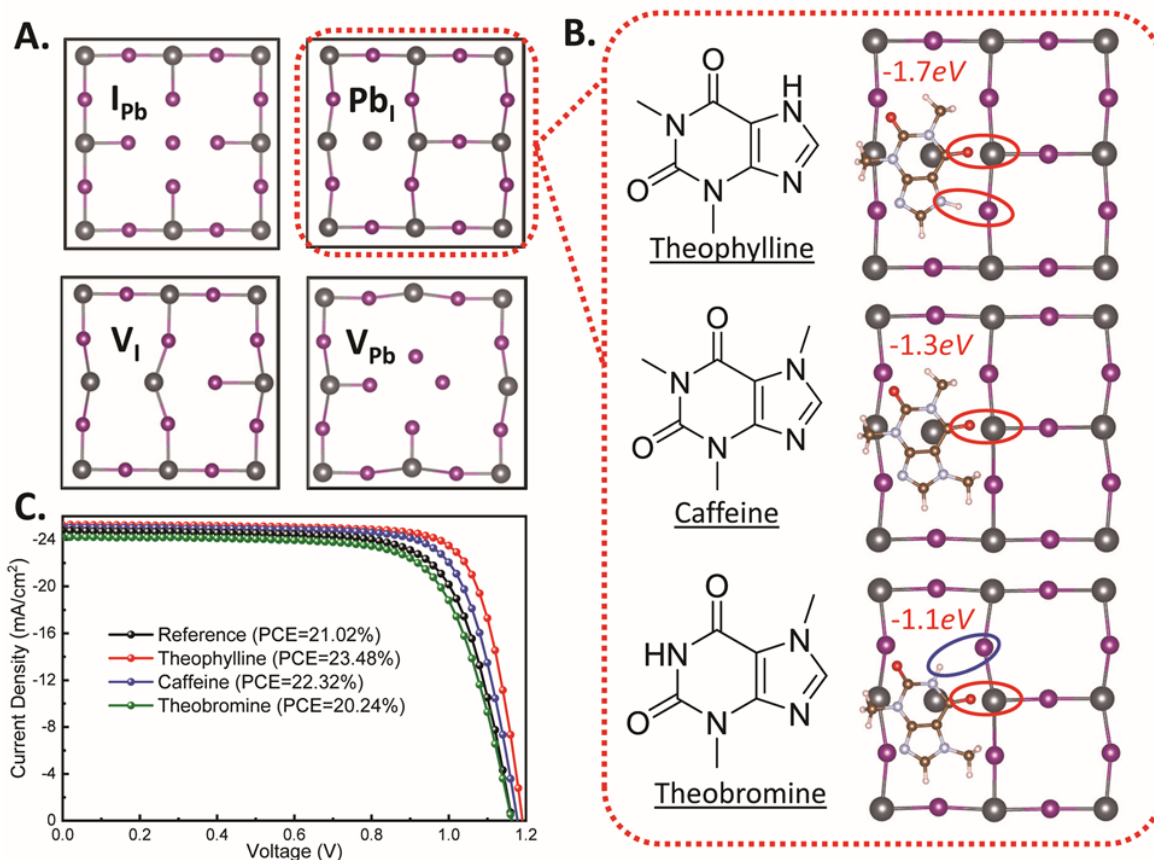


Fig. 1. Surface defect identification and constructive configuration of the C=O group in three different chemical environments. (A) Top view of the various types of surface defects. (B) Theoretical models of perovskite with molecular surface passivation of Pb_I antisite with theophylline, caffeine, and theobromine (C) $J-V$ curves of perovskite solar cells with or without small molecules treatment under reverse scan direction.

5

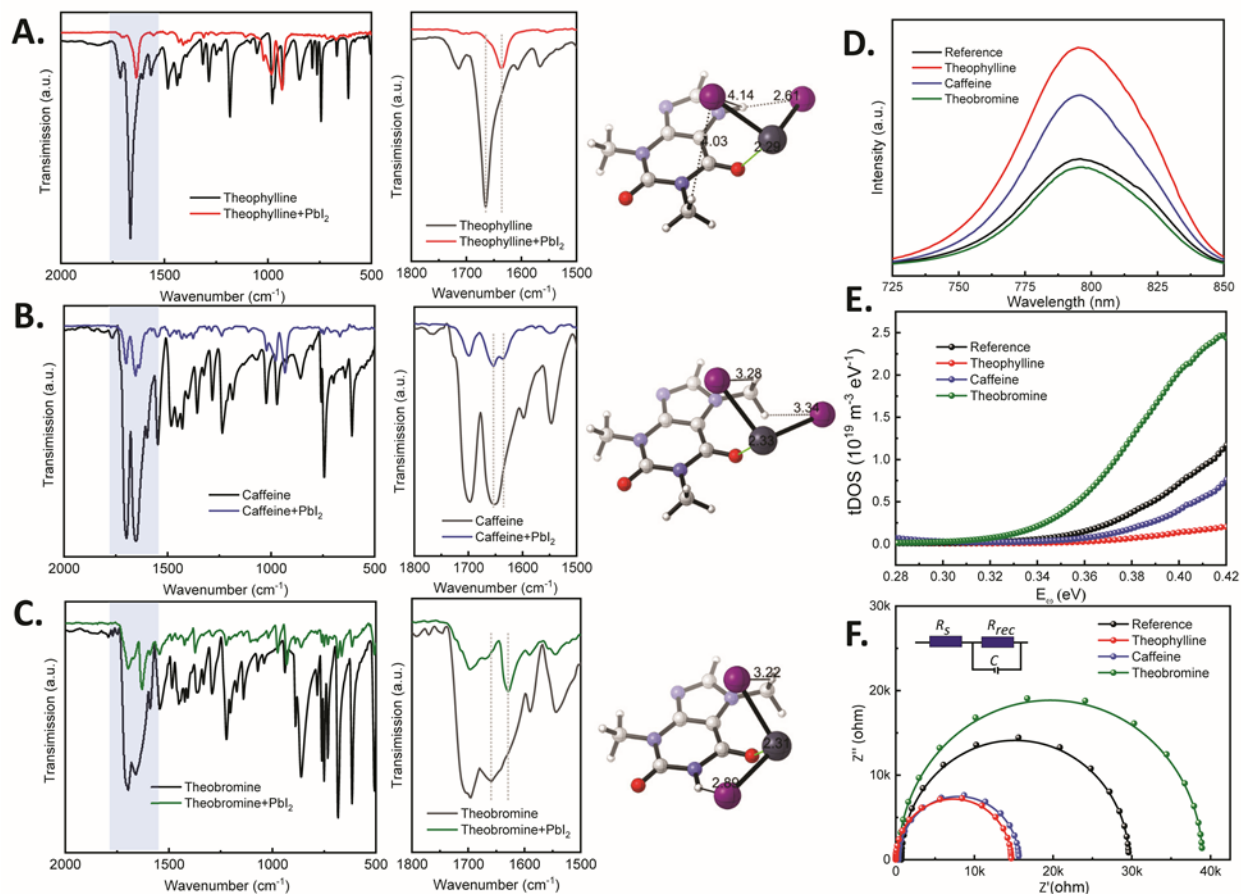


Fig. 2 Investigation of the interactions between surface defects and the small molecules.

FTIR spectra of (A) pure theophylline and theophylline-PbI₂ films; (B) pure caffeine and caffeine-PbI₂ films; (C) pure theobromine and theobromine-PbI₂ films. (D) PL spectra of perovskite films without and with small molecules treatment. (E) Trap density of states (tDOS) in perovskite solar cells with or without small molecules treatment. (F) Nyquist plots of perovskite solar cells with or without small molecules treatment measured in the dark and at corresponding open-circuit voltages.

5

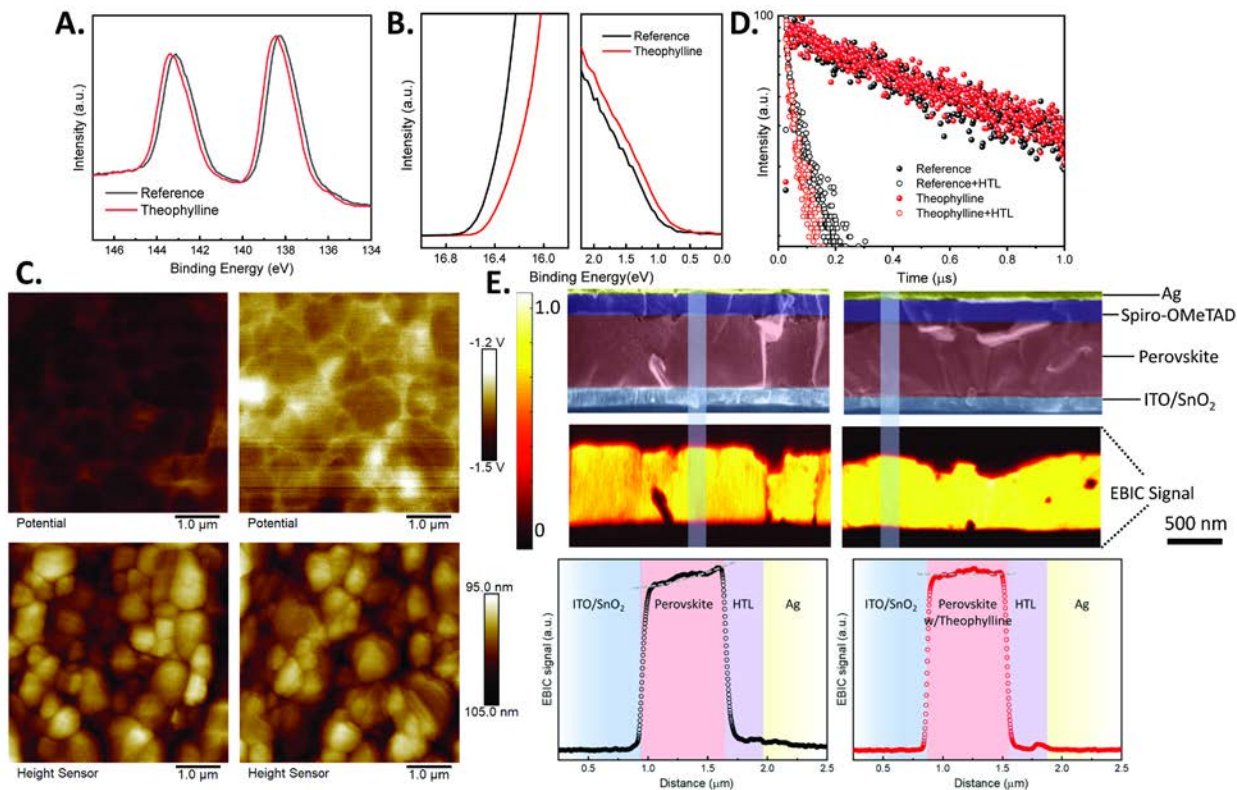


Fig. 3 Characterization of perovskite films and interfaces with theophylline treatment.

(A) XPS data for Pb 4f 7/2 and Pb 4f 5/2 core level spectra in perovskite films with or without theophylline treatment. (B) UPS spectra of perovskite films with or without theophylline treatment. (C) AFM and KPFM images of perovskite films with (right) or without (left) theophylline treatment. (D) Time-resolved PL spectra of perovskite films before and after depositing Spiro-OMeTAD without and with theophylline treatment. (E) Cross-section SEM images and the corresponding EBIC images and line profile of the perovskite solar cells with (right) or without (left) theophylline treatment.

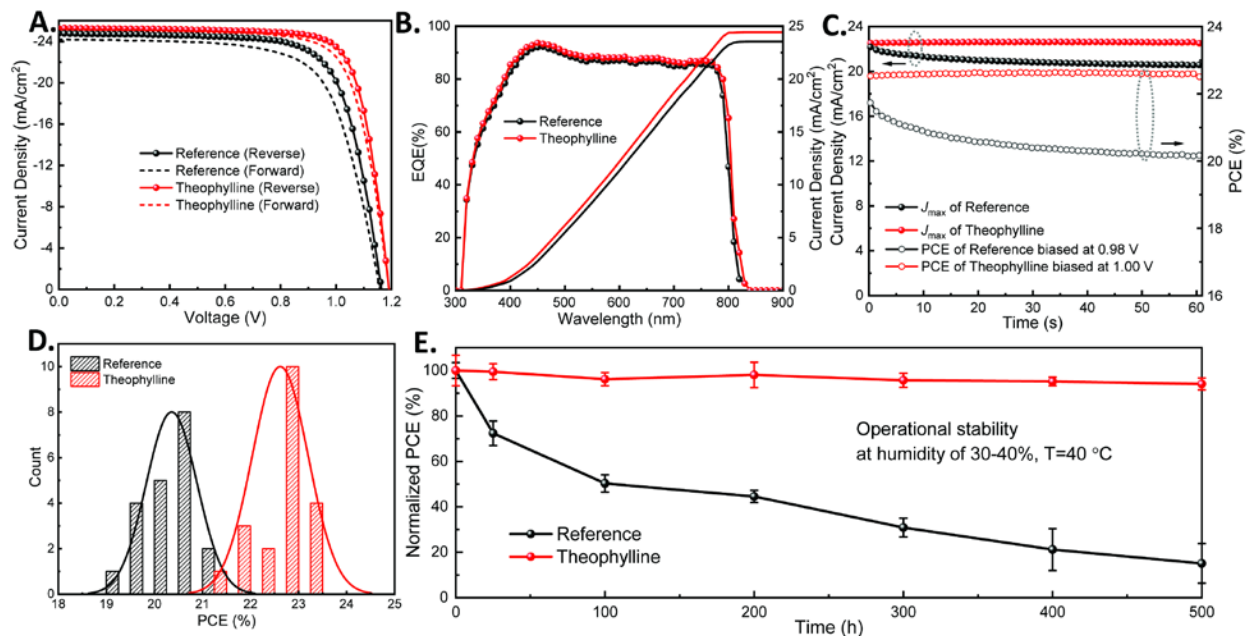


Fig. 4 Enhanced photovoltaic performance and long-term stability of perovskite solar cells with theophylline treatment.

(A) Current density–voltage (J – V) curves of perovskite solar cells with or without theophylline treatment. (B) EQE curves of perovskite solar cells with or without theophylline treatment. (C) Stabilized maximum power output and the photocurrent density at maximum power point as a function of time for the best performing perovskite solar cells with or without theophylline treatment, as shown in (A), recorded under simulated 1-sun AM1.5G illumination. (D) PCE distribution of perovskite solar cells with or without theophylline treatment. (E) Evolution of the PCEs measured from the encapsulated perovskite solar cells with or without theophylline treatment exposed to continuous light ($90 \pm 10 \text{ mW cm}^{-2}$) under open-circuit condition.